Quantifying chain reptation in entangled polymer melts: Topological and dynamical mapping of atomistic simulation results onto the tube model

Pavlos S. Stephanou, Chunggi Baig, Georgia Tsolou, Vlasis G. Mavrantzas, and Martin Kröger

Citation: The Journal of Chemical Physics **132**, 124904 (2010); doi: 10.1063/1.3361674
View online: http://dx.doi.org/10.1063/1.3361674
View Table of Contents: http://scitation.aip.org/content/aip/journal/jcp/132/12?ver=pdfcov
Published by the AIP Publishing

Quantifying chain reptation in entangled polymer melts: Topological and dynamical mapping of atomistic simulation results onto the tube model

Pavlos S. Stephanou,[1] Chunggi Baig,[1] Georgia Tsolou,[1] Vlasis G. Mavrantzas,[1,a)] and Martin Kröger[2,b)]
[1]*Department of Chemical Engineering, University of Patras and FORTH-ICE/HT, Patras, GR 26504, Greece*
[2]*Department of Materials, Polymer Physics, ETH Zürich, Wolfgang-Pauli-Str. 10, Zürich CH-8093, Switzerland*

(Received 28 August 2009; accepted 23 February 2010; published online 30 March 2010)

The topological state of entangled polymers has been analyzed recently in terms of primitive paths which allowed obtaining reliable predictions of the static (statistical) properties of the underlying entanglement network for a number of polymer melts. Through a systematic methodology that first maps atomistic molecular dynamics (MD) trajectories onto time trajectories of primitive chains and then documents primitive chain motion in terms of a curvilinear diffusion in a tubelike region around the coarse-grained chain contour, we are extending these static approaches here even further by computing the most fundamental function of the reptation theory, namely, the probability $\psi(s,t)$ that a segment s of the primitive chain remains inside the initial tube after time t, accounting directly for contour length fluctuations and constraint release. The effective diameter of the tube is independently evaluated by observing tube constraints either on atomistic displacements or on the displacement of primitive chain segments orthogonal to the initial primitive path. Having computed the tube diameter, the tube itself around each primitive path is constructed by visiting each entanglement strand along the primitive path one after the other and approximating it by the space of a small cylinder having the same axis as the entanglement strand itself and a diameter equal to the estimated effective tube diameter. Reptation of the primitive chain longitudinally inside the effective constraining tube as well as local transverse fluctuations of the chain driven mainly from constraint release and regeneration mechanisms are evident in the simulation results; the latter causes parts of the chains to venture outside their average tube surface for certain periods of time. The computed $\psi(s,t)$ curves account directly for both of these phenomena, as well as for contour length fluctuations, since all of them are automatically captured in the atomistic simulations. Linear viscoelastic properties such as the zero shear rate viscosity and the spectra of storage and loss moduli obtained on the basis of the obtained $\psi(s,t)$ curves for three different polymer melts (polyethylene, *cis*-1,4-polybutadiene, and *trans*-1,4-polybutadiene) are consistent with experimental rheological data and in qualitative agreement with the double reptation and dual constraint models. The new methodology is general and can be routinely applied to analyze primitive path dynamics and chain reptation in atomistic trajectories (accumulated through long MD simulations) of other model polymers or polymeric systems (e.g., bidisperse, branched, grafted, etc.); it is thus believed to be particularly useful in the future in evaluating proposed tube models and developing more accurate theories for entangled systems. © *2010 American Institute of Physics*.
[doi:10.1063/1.3361674]

I. INTRODUCTION

Dynamics in high molecular weight polymeric liquids is determined by topological constraints arising from chain connectivity and chain uncrossability. As discussed by Doi and Edwards[1] such a type of interaction is singular, since there is no parameter describing its strength. Its effect, however, on the viscoelastic properties of a polymeric system can be captured in a mean-field approach by the effective tube model, according to which mutual entanglements with surrounding chains restrict the number of allowed conformations of a reference chain at short times compared to those in free space. The allowed chain conformations are effectively confined in a tubelike region whose main axis is defined by the shortest path connecting the two ends of the chain and having the same topology with the chain itself relative to the constraints; this is the primitive path (PP).[1] As a result, the polymer chain moves back and forth (i.e., reptates) only along its contour with a diffusion coefficient which corresponds to the overall translation of the Rouse chain along the tube. Then, the parameter defining the strength of the topological interactions is the effective tube diameter.[1]

Through the pioneering works of de Gennes[2] and Doi and Edwards,[3] the reptation (or tube) model has been con-

a)Author to whom correspondence should be addressed. Tel.: +30-2610-997398. Electronic mail: vlasis@chemeng.upatras.gr. URL: http://lstm.chemeng.upatras.gr.
b)URL: www.complexfluids.ethz.ch.

sidered as the most successful theory of polymer physics for the description of the dynamics of entangled polymer melts and concentrated solutions. The gist of the reptation theory lies in the mathematical treatment of the highly complicated problem of how to account for the topological constraints imposed on the dynamical behavior of a chain due to its interactions with surrounding chains. A detailed description of such interactions (e.g., taking into account even small-scale fluctuations) would be practically almost intractable. With a great physical insight based on the concept of mean field, however, the reptation theory proposes representing the whole topological constraints effectively by a simple one-dimensional curvilinear "tube."[1,3] Considering that the intrinsic properties of the chain should be still represented by the Rouse model (a chain consisting of N segments with bond length b and friction coefficient ζ), in the new conceptual picture only one additional parameter is considered, the tube diameter d_t. Furthermore, instead of looking at the local dynamics of each monomer (or of each Rouse bead representing a few monomers, usually 4–6 depending on chain stiffness), the reptation theory focuses on the dynamics at a coarser level, that of the primitive chain. The underlying assumption is that the global rheological behavior of a melt of entangled polymer chains is equally well represented by the dynamics of the ensemble of their primitive chains (small-scale fluctuations being omitted) whose motion is assumed to be confined within a tubelike region around the PP, and how this changes as the chain moves (creating and destroying the ends of the PP). Therefore, within the reptation theory, the initial formidable task of the intricate full topological problem and its effect on polymer dynamics is reduced to a simpler one (the motion of the primitive chain within a tubelike region) dealing only with one single parameter related to the tube, its diameter d_t.

Key in the reptation theory is the function $\psi(s,t)$ describing the probability that the original tube segment s remains after time t. It also represents the probability that the primitive chain segment s is inside the original tube (the tube specified at time $t=0$) after time t. In general, as the chain moves back and forth, some parts of the chain leave the original tube. When a tube segment is reached by either end of the reptating primitive chain, it disappears; that is, as time passes, the original tube segment s tends to loose part of the primitive chain. The segment survival probability function $\psi(s,t)$ is central in the Doi–Edwards theory as it is behind all linear viscoelastic (LVE) properties of the polymer.[1] In particular, it defines: (i) the portion of the primitive chain that remains inside the original tube after time t through

$$\Psi(t) = \frac{1}{L}\int_0^L \psi(s,t)ds, \tag{1a}$$

where L denotes the contour length of the primitive chain, (ii) the spectrum of relaxation times, and consequently the disentanglement or reptation time τ_d, (iii) the (reduced) relaxation modulus of the polymer through

$$G(t) = G_N^0\Psi(t), \tag{1b}$$

where G_N^0 is the plateau modulus (the relation holds for times t longer than the characteristic entanglement time τ_e that segments "hit" the tube), (iv) the zero shear rate viscosity η_0 through

$$\eta_0 = \int_0^\infty G(t)dt = G_N^0\int_0^\infty \Psi(t)dt, \tag{1c}$$

(v) the steady-state compliance J_e^0 through

$$J_e^0\eta_0^2 = \int_0^\infty tG(t)dt = G_N^0\int_0^\infty t\Psi(t)dt \tag{1d}$$

and (vi) the storage $G'(\omega)$ and loss $G''(\omega)$ moduli through

$$G'(\omega) = \omega\int_0^\infty G(t)\sin(\omega t)dt = G_N^0\omega\int_0^\infty \Psi(t)\sin(\omega t)dt \tag{1e}$$

and

$$G''(\omega) = \omega\int_0^\infty G(t)\cos(\omega t)dt = G_N^0\omega\int_0^\infty \Psi(t)\cos(\omega t)dt, \tag{1f}$$

respectively.

Despite the success of the original (Doi–Edwards) reptation model to elucidate a great deal of puzzling phenomena unique to entangled polymers[1–4] and biopolymers,[5,6] its quantitative predictions were not convincing in all aspects.[7,8] For example, for the particular case where the function $\psi(s,t)$ is analytically given by the simple formula $\psi(s,t) = \Sigma_{p:\text{odd}}(4/p\pi)\sin(p\pi s/L)\exp(-p^2t/\tau_d)$ as in the original Doi–Edwards theory,[1] the resulting expressions for the zero shear rate viscosity η_0 and the chain center-of-mass self-diffusion coefficient D_G suggest that $\eta_0 \sim N^3$ and $D_G \sim N^{-2}$, which do not agree completely well with experimental data.[7,8] This motivated refinements in the theory through consideration of additional phenomena and mechanisms present in real systems that had been neglected at first place. Indeed, two important mechanisms addressed by modern tube theories are those related to contour length fluctuations (CLFs) of the primitive chain and constraint release (CR) caused by the movement of surrounding chains.[7] While the latter considers cooperative phenomena between chains, the former can be characterized as a single-chain phenomenon which becomes negligible for infinitely long chain lengths (but it is not negligible for moderate-to-long chain lengths that are typically encountered in practical applications). Various models have been proposed to account for these effects (e.g., the calculation of CLFs on the disentanglement time can be analyzed as a first passage problem in multidimensional phase space or through a variational approach[9–11]), resulting in significant improvements[7,12,13] of the theory while further developments are still in progress.

Despite these further efforts to improve on the tube theory, two fundamental issues related to the initial idea (that could provide a microscopic foundation of such a highly successful phenomenological model) have remained unre-

solved over the years: (a) how to analyze the topological state of a polymeric liquid in terms of PPs, and (b) how to systematically obtain the function $\psi(s,t)$, which is considered as the central element in all tube models. Computer simulations are regarded here as the best tool (maybe the only one) with the potential to address the two questions, since they can provide us with the full phase-space information (positions and velocities) in time at any level of the description needed. To this, by implementing the tube model idea into a simulation code for dense melts of bead-spring polymer chains with variable intrinsic stiffness (chain segments represented as spheres with short-ranged excluded-volume interactions and connected via springs to form model polymer chains) and analyzing their topological state in terms of PPs, Everaers *et al.*[14] provided practically the first solution to question (a) above, with remarkable quantitative predictions for the plateau modulus for all major classes of synthetic polymers (polyolefins, polydienes, polyacrylates, and polycarbonate). They achieved this through an approach that minimizes the energy of the system by slowly cooling down its temperature to 0 K while keeping chain ends fixed in space and maintaining only interchain excluded volume interactions. Without thermal fluctuations and with all intrachain excluded volume interactions being disabled, chains are pulled taut without crossing (but by simply sliding past) each other. Independent efforts by Kröger and co-workers[15,16] and Tzoumanekas and Theodorou[17] employing geometrical rather than dynamical operations to calculate the PP helped gain additional insight into the statistical properties of the PP mesh (entanglement length, PP length, PP potential, etc.) for a number of linear polymers and compare against analytic expressions derived from statistical mechanics for a chain that is random walk with randomly scattered entanglements.[18]

We provide here an answer to question (b), namely the systematic calculation of the function $\psi(s,t)$ which makes the connection between primitive chain dynamics on one hand and macroscopic viscoelastic properties and theoretical models on the other hand, for an entangled polymeric liquid. We achieve this by introducing a methodology that reduces trajectories from detailed (and very long) atomistic molecular dynamics (MD) simulations to trajectories of PPs, followed by a geometric and dynamical mapping onto the tube model. The power of the new method is demonstrated in direct comparisons of the results obtained from the computed $\psi(s,t)$ curves for the viscoelastic properties of three kinds of moderately entangled polymer melts (linear polyethylene, linear *cis*-1,4-polybutadiene (PB), and linear *trans*-1,4-PB) with available experimental rheological data and the predictions of theoretical models.

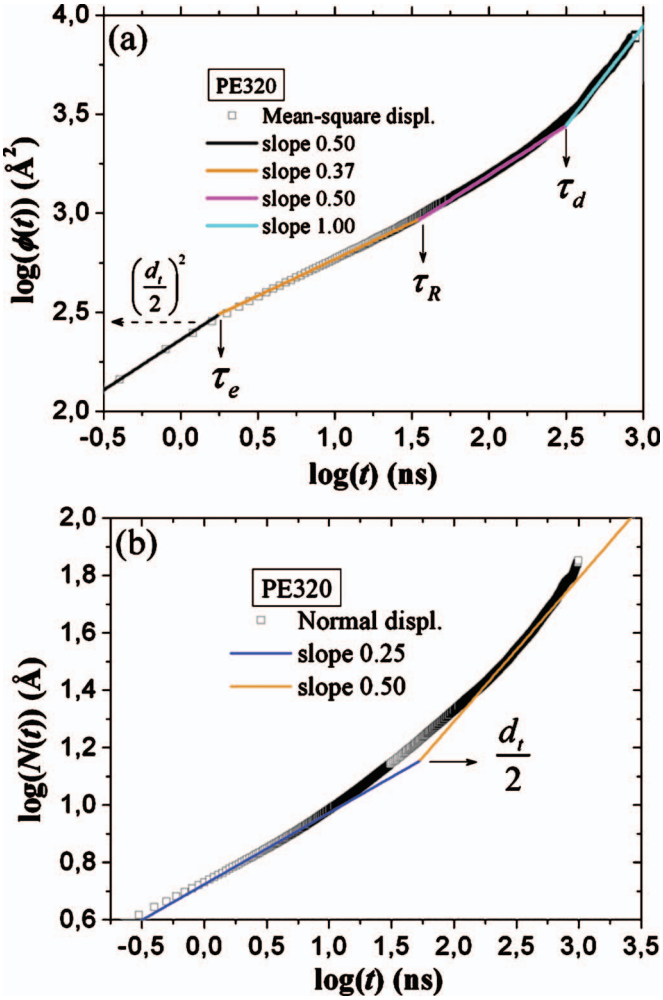

FIG. 1. (a) Calculation of the tube diameter d_t based on the atomistic segmental msd of the innermost chain segments $\phi(t)=\langle(\mathbf{r}_n(t)-\mathbf{r}_n(0))^2\rangle$ vs time t. Four distinct regimes are seen in the figure exactly as predicted by the reptation theory (Ref. 1). The tube diameter is estimated as $d_t=2\sqrt{\phi(t^*)}$ where $\phi(t_*)$ is registered at $t=t^*$ when the slope of $\phi(t)$ starts to change as it leaves the initial $t^{1/2}$ regime to enter the next $t^{1/4}$ regime. (b) Calculation of the tube diameter d_t based on the time displacement of the primitive chain segments orthogonal to the initial PP (the PP at time $t=0$) vs time t. As the segments "feel" the tube constraints, a break in their displacement appears. The average value of the perpendicular displacement at the break point (which we locate by fitting the curve before and after it with straight lines) provides a reasonable estimate of $d_t/2$.

II. COMPUTATIONAL METHODOLOGY

Our procedure entails the following five steps:

(1) We determine the entanglement time τ_e, the Rouse time τ_R, and the disentanglement time τ_d by analyzing the segmental mean square displacement (msd) versus time t [see Fig. 1(a)] obtained directly from the atomistic simulations by observing the three characteristic breaks denoting the onset of tube constraints on segmental diffusion, the Rouse-like diffusion combined with tube constraints, and the passage from the Rouse-like diffusion to reptation dynamics.[1] The results obtained for three types of model polymers linear PE, *cis*-1,4-PB, and *trans*-1,4-PB) are reported in Table I.

(2) We perform the PP analysis of the atomistic trajectory with the recently proposed Z1 code[15,16,19] to obtain the dynamic trajectory of primitive chains: such a reduction provides not only the statistical properties (average and standard deviation or fluctuation) of the underlying topological network but also the position of each kink (entanglement) point along the path. The algorithm considers primitive paths as thin lines connecting the two ends of a polymer chain that are considered as fixed in space. The primitive paths are obtained under

TABLE I. Results for the density ρ, the entanglement time τ_e, the disentanglement time τ_d, the tube diameter d_t as obtained from the methodology presented in this work, and the step length a_s of the PP estimated as $a_s = \langle R^2 \rangle / \langle L \rangle$, for the simulated polymer melts. The atomistic MD simulations were performed at $T=450$ K and $P=1$ atm for the PE systems and $T=413$ K and $P=1$ atm for the PB systems.

System[a]	ρ (g/cm^3)	τ_e (ns)	τ_d (ns)	d_t [b] (Å)	a_s (Å)
PE320 (32)	0.767	2.1 ± 0.5	316 ± 32	33 ± 4	37 ± 4
PE400 (16)	0.768	2.9 ± 0.4	489 ± 25	33 ± 7	39 ± 7
PE500 (16)	0.769	2.8 ± 0.4	1042 ± 46	32 ± 6	43 ± 9
PB-*trans*320 (32)	0.837	3.2 ± 0.7	264 ± 34	26 ± 6	39 ± 5
PB-*trans*400 (32)	0.838	3.1 ± 0.5	355 ± 25	26 ± 4	38 ± 5
PB-*cis*320 (32)	0.863	1.8 ± 0.2	138 ± 18	32 ± 6	38 ± 5
PB-*cis*400 (32)	0.865	2.3 ± 1.0	256 ± 24	29 ± 4	39 ± 4
PB-*cis*800 (24)	0.864	2.3 ± 0.5	1255 ± 50	30 ± 4	43 ± 5

[a]Number in parenthesis gives the number of chains.
[b]Tube diameter values calculated either as $d_t = 2\sqrt{\phi(t^*)}$ where $\phi(t^*)$ denotes the segmental msd at the time $t = t^*$ where the slope of $\phi(t)$ begins to change as segments leave the initial $t^{1/2}$ regime (in a log-log plot) and enter the $t^{1/4}$ regime, or from the perpendicular displacement of the PP segments at the time marking the onset of tube constraints on their motion. The two methods gave approximately the same result, thus only one value of tube diameter per simulated system is reported in the table.

the constraints of chain connectivity and uncrossability through a set of special geometric operations designed to minimize the contour length of the multiple disconnected path (i.e., the contour length summed over all individual PPs) simultaneously for all chains present in the simulation cell.

(3) We determine the tube diameter d_t with two methods: (a) by analyzing the segmental msd versus time as obtained directly from the atomistic simulations [Fig. 1(a)], and (b) by monitoring the displacement of primitive chain segments orthogonal to the initial PP [Fig. 1(b)]. In the first case, we follow the segmental msd $\phi(t) = \langle (\mathbf{r}_n(t) - \mathbf{r}_n(0))^2 \rangle$ in time and we estimate the tube diameter as $d_t = 2\sqrt{\phi(t^*)}$ where $\phi(t^*)$ is registered at $t = t^*$ where the slope of $\phi(t)$ changes as it leaves the initial $t^{1/2}$ regime (in a log-log plot) to enter the $t^{1/4}$ regime (see p. 213 in Ref. 1 for details). Here, $\mathbf{r}_n$ denotes the position vector of the nth monomer, and only monomers close to the middle of chains are included in the calculations to avoid chain free-end effects. In the second case, we monitor the displacement of primitive segments orthogonal to the initial PP: The value of the perpendicular displacement at the intersection of the curves marking the onset of tube constraints on their motion is taken as the average tube radius [see Fig. 1(b)]. The results obtained with the two methods for the simulated polymers are practically identical (within the statistical uncertainty), thus in Table I only their average value is reported.

(4) Knowing d_t and using the mapped time trajectory of primitive chains, we calculate $\psi(s,t)$ as follows: (a) First, we geometrically construct the initial (corresponding to time $t=0$) tube around each entanglement strand for a given primitive path [see Fig. 2(a)] by approximating it with the space of a small cylinder around it having the same axis as the entanglement strand itself and a diameter equal to the estimated average tube diameter d_t [see Fig. 2(b)]. (b) We properly place segments along the contour of the primitive chain at equidistant points on the normalized $[0,1]$ interval by taking into account that each such chain is made up of rectilinear strands. Clearly, this does not alter the instantaneous value of the chain contour length; on the other hand, working on the normalized $[0,1]$ interval greatly facilitates the computations because the number of kinks (entanglements) along a given chain changes with time in the course of the MD simulation (and the same happens with the contour length). In this work, 101 points were chosen to be placed along each primitive chain and monitored in time, implying that the distance between any two consecutive primitive chain segments is 0.01 in dimensionless units. By maintaining special lists, a one-to-one correspondence between a segment s in the normalized $[0,1]$ interval and true coordinate in the dimensional $[0,L]$ interval is established, which is always available in the computations together with the information about the entanglement strand to which the dimensionless arc-length coordinate s should correspond to at any time instance t (thus, also its true position with respect to the confining tube). This is important because it helps avoid errors arising from the fact that entanglements are continuously being created and lost or from the strong CLFs characterizing the (moderately entangled) systems studied here. (c) We monitor the displacement of each segment s at times $t>0$ to determine whether the segment has, or has not, escaped the initial tube. To this, we measure its shortest spatial distance x from the entire initial PP [see Fig. 2(b)]. Since a segment can escape either perpendicularly or longitudinally, we set two criteria: (i) If $x(s) > d_t/2$, we consider this segment as having escaped the initial tube perpendicularly and we set $\psi(s,t)=0$, (ii) if $x(s) < d_t/2$, the segment has not escaped the tube perpendicularly, but we further check if it has escaped it longitudinally along the curvilinear axis of the tube. When applying the two criteria, special care should be

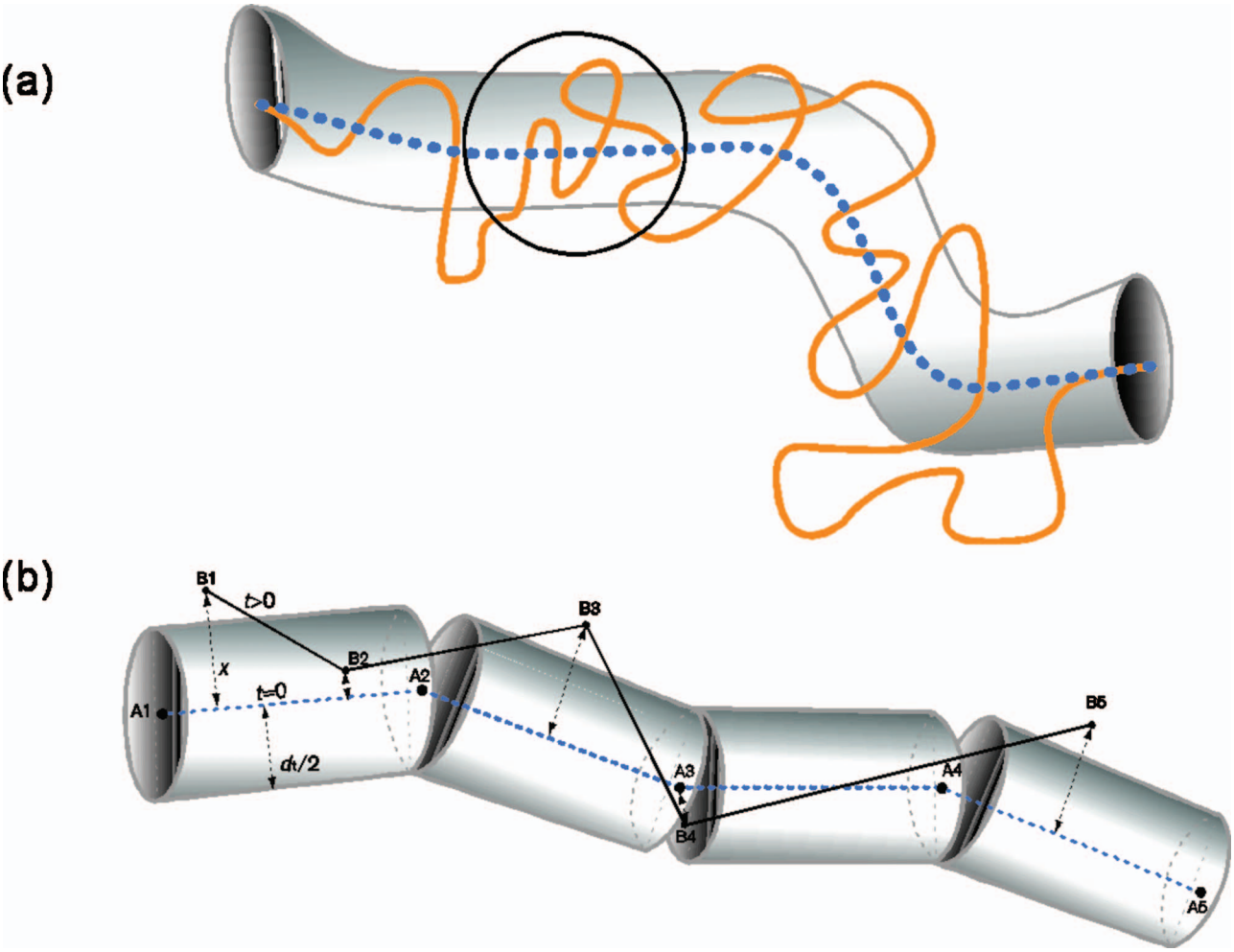

FIG. 2. Schematic of the tube construction around a chain PP for the computation of the function $\psi(s,t)$. Shown in part (a) of the figure are an atomistic chain (in light orange), its PP (in blue), and the tube constraining the lateral motion of the chain, all at time $t=0$. The tube is constructed piece-by-piece, see part (b) of the figure where we have zoomed at a small portion of the original primitive chain (the part labeled A1-A2-A3-A4-A5), by visiting each entanglement strand along the PP at $t=0$ and building a small cylinder around it which has the same axis as the entanglement strand itself and a diameter equal to the computed average tube diameter d_t. The function $\psi(s,t)$ is obtained by monitoring the primitive chain at times $t>0$ (when, e.g., the part of the chain labeled A1-A2-A3-A4-A5 in Fig. 2(b) has moved to the new conformation labeled B1-B2-B3-B4-B5), computing the perpendicular displacement x at primitive chain segment s, and comparing it to the tube radius $d_t/2$. We also check if segment s has escaped laterally (i.e., if it has moved to the left of the very first small cylinder or to the right of the very last small cylinder).

taken at the kink points where two cylinders intersect each other: In this case, if a segment s is found outside the space spanned by the two cylinders on the right and the left of the kink (i.e., in the space where the two cylinders do not overlap), then the criteria are applied by checking the distance x of the primitive chain segment directly from the kink [this is, e.g., the case with primitive chain segment B4 in Fig. 2(b)].

The above criteria capture correctly the dynamics of PP segments at rather short time scales when the segment s is either inside the original tube or just outside. At larger time scales, we need to impose an additional criterion on $\psi(s,t)$, since chains may return back to their original tubes through self-diffusion or thermal fluctuations. To capture this, we have been guided by Doi[20] who proposed a methodology for computing the fluctuation in the tube radius by considering its mean value, a_t, as the average distance of segments of one chain from their nearest segments in other chains. More precisely, Doi[20] proposed that $a_t=\langle r\rangle=\int_0^\infty drQ(r;\sigma)r$, where $Q(r;\sigma)dr$ denotes the probability that the nearest segments of others chains lie in the domain r and $r+dr$; this is a function of the dimensionless parameter σ defined as $\sigma=(\langle R^2\rangle/6)^{1/2}/l$ where $\mathbf{R}$ denotes the chain end-to-end vector and l the intermolecular separation given approximately by $l=c^{-1/3}$ where c is the polymer number density. Based on the above considerations, one can compute an estimate of the fluctuation in the tube radius through $\langle\Delta r^2\rangle/a_t^2=(\langle r^2\rangle-\langle r\rangle^2)/a_t^2=(\langle r^2\rangle/\langle r\rangle^2)-1$. For the systems dealt with in the present work, $\langle\Delta r^2\rangle$ comes out to be approximately equal to a_t^2 (i.e., to the square of the average tube radius), implying that the fluctuation in the tube radius is practically equal to its average value. Motivated by this result, our criterion for the perpendicular escape of segments that have moved a distance larger than the tube radius, $d_t/2$, is stated *more precisely* as follows: If the total perpendicular distance is less than two times the tube radius,

then although we set $\psi(s,t)=0$, we still allow the segment to return back to the original tube at later times (i.e., the segment in this case is assumed to fluctuate in and out the tube in the vicinity of its outer surface). If, however, the total perpendicular distance is greater than two times the tube radius, then the segment is considered as having *completely* escaped the original tube; in this case, we set $\psi(s,t)=0$ *and* we do not allow the segment to return back to its original tube, thus we also set $\psi(s,t)=0$ for all subsequent times. This is to indicate complete relaxation of the stress imposed by the initial tube. That is, as far as perpendicular escape is concerned, we distinguish eventually between three cases: (a) If $x(s)<d_t/2$ then $\psi(s,t)=1$; (b) If $d_t/2<x(s)<d_t$, then $\psi(s,t)=0$ *but* the segment can return back to the original tube; and (c) If $d_t<x(s)$ then $\psi(s,t)=0$ *and* the segment cannot return back to the original tube, thus $\psi(s,t)=0$ for all subsequent times as well. Perpendicular escape is very important to consider, especially in the present study, in the light of the relatively small length of the simulated (moderately entangled) melts: driven by CR, this is an important relaxation mechanism for these systems.

(5) The function $\psi(s,t)$ for each segment s is obtained by using the results of step (4) and averaging over all chains in the system as follows. The MD simulation provides us with the system trajectory at the level of individual atoms (carbon atoms and hydrogens), at all times t. By invoking the Z1 code, the atomistic snapshot at any time t is transformed into a snapshot of primitive chains. For a given chain, we make use of the criteria discussed in step (4) to decide about the value of $\psi(s,t)$. For example, for the primitive chain segments B1, B2, B3, B4, and B5 shown in Fig. 2(b), at the given time t for which the snapshot is illustrated, we have that: $\psi(B1,t)=0$, $\psi(B2,t)=1$, $\psi(B3,t)=0$, $\psi(B4,t)=1$, and $\psi(B5,t)=0$. Then we repeat the calculations for all chains and we take their average for the given segment s. To improve statistics, we further make use of the technique of multiple time origins. Eventually, for the given segment s in the normalized interval [0,1] along the contour of the primitive chain and for the given time interval t, $\psi(s,t)$ is calculated as the mean value (the average) of all values 1 and 0 collected for all chains present in the system and for all possible time origins analyzed. The converged result is the desired survival probability $\psi(s,t)$ reported in the paper. Since the polymer chains possess head-to-tail symmetry, statistics is further improved by restricting (without loss of generality) the primitive path analysis to $s\in[0,1/2]$ and using $\psi(s,t)=\psi(1-s,t), \forall s\in[0,1/2]$ and $\forall t$.

A few points about the methodology outlined in steps (1) through (5) above are in place here in order to make clear its distinction from theoretical approaches to the reptation problem:

(a) It borrows only the most fundamental idea of the tube model, namely, the postulate that entanglements or topological constraints can be equally represented by a mean-field effective tube of a certain width or diameter surrounding the polymer molecule, and chain relaxation occurs as the chain escapes from the tube through reptation and *any* additional mechanism such as CLF and CR. In essence, following Rubinstein and Helfand,[21] our view of the primitive chain and of its confining tube is the one which considers a time exposure of the reference chain (in the sea of the rest of the chains): A time averaged single molecule density pattern would lead then to a curve with a characteristic width. The curve or line or ridge which follows the maximum value of this averaged pattern defines the primitive chain while its width (which is representative of the fluctuations orthogonal to the primitive chain) defines the effective tube diameter. More precisely, in the present study, the primitive chains are constructed not as the loci of the maximum values of the time-averaged molecular density patterns but as the shortest paths connecting the two chain ends (which are assumed to be fixed in space) which, further, are consistent with the topology imposed on each chain by the uncrossability constraints due to surrounding chains. However, we do make use of Rubinstein–Helfand's view of the confining tube as representing the characteristic width of this averaged molecular density pattern given the underlying entanglement network.

(b) It *automatically accounts for CLF and CR phenomena*, since the primitive chains are computed directly from the *instantaneous* trajectories of the simulated polymers by taking into account at any time instant the *current* topological constraints, as atoms move in time in the course of the MD simulation according to Newton's equations of motion at the specified conditions of temperature and pressure. This is the strongest point of the present approach: It extracts information about the relaxation mechanisms in entangled polymers by projecting dynamic data obtained at the most fundamental level (the atomistic) to a coarser level (that of primitive chains). As such, the method can be used in the future to evaluate modern tube theories proposed to account for a hierarchy of effects in entangled polymer melts either at equilibrium or under flow.

(c) Eventually, the function $\psi(s,t)$ will be used to compute the viscoelastic properties of the melt, such as the modulus of relaxation, the zero shear rate viscosity, and the spectra of loss and storage moduli, by making use of Eqs. (1a)–(1d) and (1f) above. From a statistical mechanics point of view, the relaxation modulus is given by the time autocorrelation function of the non-diagonal elements of the instantaneous stress tensor $\boldsymbol{\sigma}(t)$

$$G(t)=\frac{V}{k_BT}\langle\sigma_{\alpha\beta}(t)\sigma_{\alpha\beta}(0)\rangle, \quad \alpha\neq\beta=x,y,z, \tag{2}$$

where V denotes the system volume, T the temperature, and k_B is the Boltzmann constant. In principle, the instantaneous stress tensor $\boldsymbol{\sigma}(t)$ needed in Eq. (2) is obtainable directly from the MD simulations through the virial theorem. Unfortunately, because of the strong

fluctuations in the values of the off-diagonal components of $\boldsymbol{\sigma}(t)$, extremely long configurational averaging is required to calculate $G(t)$ with the required accuracy. In the literature, calculations of $G(t)$ for detailed, fully atomistic models of polymers based on the above expression have been reported by Mondello and Grest,[22] but only for short alkanes. Harmandaris *et al.*[23] have also used Eq. (2) to directly calculate $G(t)$ for short polymer melts (such as a C_{24} and a C_{78} polyethylene melt) but that was possible only for times less than 10 ps; for longer times, the statistical noise in the calculated $\langle \sigma_{\alpha\beta}(t)\sigma_{\alpha\beta}(0)\rangle$ time autocorrelation function values was too large to allow for any meaningful results to be obtained. The present methodology allows one to overcome numerical difficulties associated with the use of Eq. (2) by reconstructing $G(t)$ for times t referring to the entangled state (i.e., $t > \tau_e$) with the help of the $\psi(s,t)$ function.

(d) The value of the plateau modulus G_N^0 needed in Eqs. (1a)–(1f) can be estimated by using the following expression:[1]

$$G_N^0 = \frac{4}{5}\frac{\rho RT}{M}\frac{\langle L\rangle}{a_s}, \tag{3}$$

where a_s denotes the step length of the primitive path.

(e) Although we cannot directly apply the exact expression, Eq. (2), at the atomistic level for the calculation of $G(t)$, one can make use of a simplified formula for the stress, namely[1,3,7]

$$\sigma_{\alpha\beta} = \frac{1}{V}\sum_{i=1}^{N_{\text{chain}}}\sum_{a=1}^{Z} r_{ia,\alpha}F_{ia,\beta} = \frac{3k_BT}{V\langle R^2\rangle}\sum_{i=1}^{N_{\text{chain}}} L_i\sum_{a=1}^{Z} r_{ia,\alpha}u_{ia,\beta}, \quad \alpha \neq \beta = x,y,z \tag{4}$$

relying on the entropy loss due to applied stress. Its origin lies on rubber elasticity theories according to which the stress arises from the anisotropic orientation of the elastically active segments and is dominated by the entropy associated with their orientation. It is derived by assuming that the tension along every entanglement segment is $\boldsymbol{F}_{ia} = (3k_BT/\langle R^2\rangle)L_i\boldsymbol{u}_{ia}$ and by counting strands transferring tension across entanglement points.[1,7] In Eq. (4), $\mathbf{u}$ denotes the unit vector tangent to the primitive contour containing a chain segment of end-to-end length approximately equal to the tube diameter. But we should keep in mind that this is only an approximate expression: it is derived by employing a coarse-grained representation for the polymer chains, it is purely entropic in origin, and it accounts only for contributions from the slow degrees of freedom since only length scales larger than the tube diameter are considered.[7]

(f) If CR effects are neglected, then according to the Doi–Edwards theory,[1] one can compute the function $\psi(s,t)$ also from the time correlation function of the tangent vectors $\mathbf{u}$ at primitive path segments s and s' after time t. That is, if we define the correlation function

$$\psi'(s,t) = \frac{1}{a_s}\int_0^L \langle \mathbf{u}(s,t)\cdot\mathbf{u}(s',0)\rangle ds' \tag{5a}$$

then, in the absence of CR we have that $\psi(s,t) = \psi'(s,t)$. In that case (i.e., in the absence of CR) by integrating the function $\psi'(s,t)$ with respect to time t, it is easy to see that the function $\Psi'(t) = (1/L)\int_0^L \psi'(s,t)ds$ defining the average portion of the primitive chain that remains inside the original tube after time t should be equal to the time autocorrelation function of the chain end-to-end vector $\mathbf{R}$

$$\Psi'(t) = \frac{\langle \mathbf{R}(t)\cdot\mathbf{R}(0)\rangle}{\langle R^2\rangle}. \tag{5b}$$

That is, if CR effects are neglected, then not only $\psi(s,t) = \psi'(s,t)$ but also $\Psi(t) = \Psi'(t)$. However, in our analysis, CR effects are directly (and automatically) accounted for, so for the polymeric systems simulated here we expect the function $\psi(s,t)$ from the direct PP analysis to be different from the function $\psi'(s,t)$ computed from Eq. (5a) and that also $\Psi(t) \neq \Psi'(t)$. In fact, since CR accelerates stress relaxation (by removing topological obstacles along the chain) without affecting the decay of the chain end-to-end vector autocorrelation, $\psi(s,t)$ and $\Psi(t)$ should decay faster than $\psi'(s,t)$ and $\Psi'(t)$, respectively. We confirm all these in Sec. III below.

III. RESULTS AND DISCUSSION

We have applied our methodology to atomistic MD simulation trajectories accumulated in the recent past[24,25] for a number of model linear PE and PB melts: C_{320}, C_{400}, and C_{500} PE melts (denoted as PE320, PE400, and PE500, respectively), C_{320}, C_{400}, and C_{800} *cis*-1,4-PB (denoted as PB-*cis*320, PB-*cis*400 and PB-*cis*800, respectively) and C_{320} and C_{400} *trans*-1,4-PB melts (denoted as PB-*trans*320, and PB-*trans*400, respectively). All PE and *trans*-1,4-PB systems and the PB-*cis*800 system are strictly monodisperse (polydispersity index $I=1$), whereas the PB-*cis*320 and PB-*cis*400 systems are slightly polydisperse ($I=1.08$ and $I=1.05$ for PB-*cis*320 and PB-*cis*400, respectively). The atomistic data have been obtained through isothermal-isobaric (*NPT*) MD simulations at $T=450$ K and $P=1$ atm for the PE melts, and at $T=413$ K and $P=1$ atm for the PB melts. To improve the statistics of the configurational averages, sufficiently long trajectories (from 750 ns up to 4 μs) were accumulated for each system. For more details on the atomistic MD simulations, we refer interested readers to Refs. 24 and 25.

In Table I, we have collected our data for the density ρ, the entanglement time τ_e, the disentanglement time τ_d, and the average tube diameter d_t for all studied systems. Despite the independent measurements for each one of them, the results appear to be physically very reasonable (e.g., d_t and τ_e are approximately chain-length independent within the statistical uncertainty). In the last column of Table I, we also report values for the step length a_s of the primitive path as calculated by using $a_s = \langle R^2\rangle/\langle L\rangle$, where L denotes the instan-

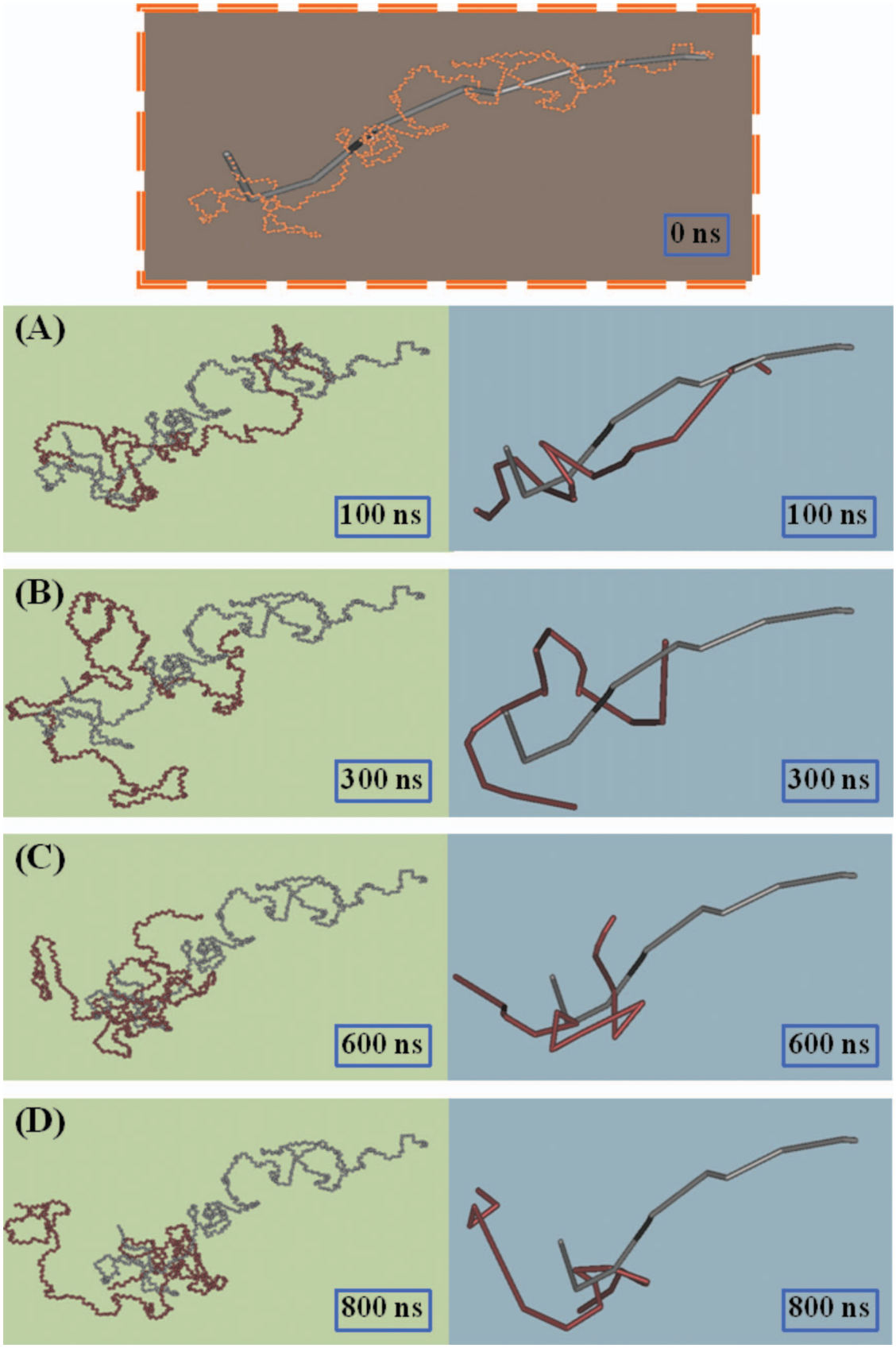

FIG. 3. A reptating chain. On the left we show how the atomistic configuration of a single chain from the simulations with the PE500 system changes with time and on the right the corresponding changes in its PP. Atomistic and primitive chain configurations at $t=0$ are also shown. The primitive chain pictures reveal that the polymer chain moves mainly back and forth its main contour, which brings more and more segments out of the original tube. Chain ends escape first and middle segments follow.

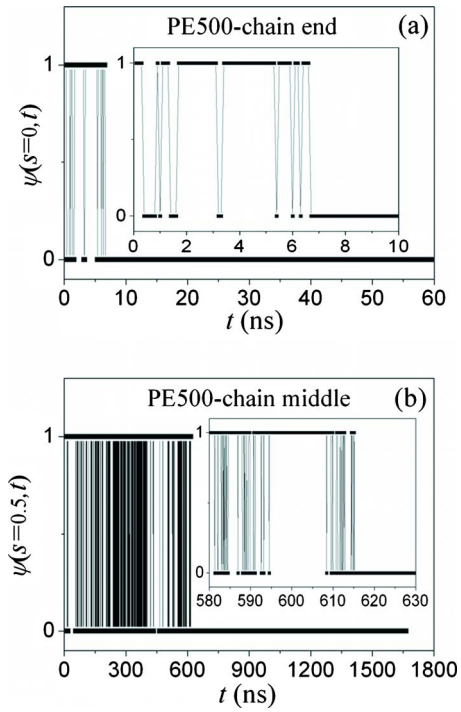

FIG. 4. Instantaneous values of the $\psi(s,t)$ function for a randomly selected PE500 chain. (a) Dynamics of end segments ($s=0$ and $s=1$). (b) Dynamics of the middle segment ($s=0.5$).

taneous value of the contour length of the primitive chain. Although d_t and a_s in tube models are typically assumed to have about the same value (although Öttinger[26] argues that a_s should be twice as large as d_t for the Porod–Kratky chain, by making use of a competing-spring coarse-grained model), their quantitative relation is still unknown. For the moderately entangled melts investigated here, our results show that a_s is approximately 15%–30% larger than d_t. We further note that the results for the step length are consistent with those obtained by applying the formula suggested by tube theories,[1] namely $a_s^{\text{theory}}=(l_0 l_K N_e)^{1/2}$ where l_0 is the equilibrium carbon-carbon length, l_K the Kuhn length (calculated as the ratio of the average end-to-end distance and the maximum length of the chain, $\langle R^2\rangle/R_{\max}$) and N_e the entanglement length. The values used here are: $l_0=1.54$ Å, $l_K=13$ Å (Refs. 27 and 28) and $N_e=68$ (Refs. 27 and 29) giving $a_s^{\text{theory}}=36.9$ Å for all PE systems, and $l_0=1.54$ Å, $l_K=9.4$ Å,[28] and $N_e=130$ (Ref. 28) (corresponding to 1,4-PB systems with the composition of 50/40/10 *trans/cis/vinyl*) giving $a_s^{\text{theory}}=43.4$ Å for all *trans*-1,4-PB systems. Alternatively, one can make use of the l_K and N_e values obtained directly from the topological analysis of the atomistic trajectories carried out in the course of this work: $l_K=14.8\pm2.2$ Å and $N_e=76\pm11$ giving $a_s^{\text{theory}}=41.6\pm6.2$ Å for PE, $l_K=10.0\pm1.5$ Å and $N_e=119\pm15$ giving $a_s^{\text{theory}}=42.7\pm5.9$ Å for *trans*-1,4-PB, $l_K=8.9\pm1.3$ Å, and $N_e=144\pm19$ giving $a_s^{\text{theory}}=44.4\pm6.0$ Å for *cis*-1,4-PB. Overall, the agreement between theoretical and simulation results for a_s is fairly good.

In Fig. 3, we show successive pictures of the instantaneous conformation of a C_{500} PE chain taken from the simulations with the PE500 system in time intervals of 100–300 ns. For clarity, only the configuration of one chain (out of 16 present in the simulation box) is shown. We can see on the left the changes at the atomistic level and on the right the changes at the coarse grained level (the primitive chain, where only the slow degrees of freedom, i.e., length scales larger than the tube radius, are considered) as extracted directly from the Z1 code. The primitive chain consists of rectilinear entanglement strands with strongly varying lengths coming together sharply at the nodal or kink points, and fluctuates mainly longitudinally by moving continuously back and forth along its contour. It is evident from the figure, however, that this reptative motion is not the only mode of dynamics of the primitive chain. The number of kinks along the chain contour also fluctuates, indicative of both CLF and CR effects. The CR effects give rise to the development and relaxation of local transverse modes along the contour which cause parts of the chain to venture outside the average tube surface for certain periods of time (before they escape completely). These are further enhanced by fast local fluctuations in the direction perpendicular to the main primitive chain orientation due to thermal motion. Overall, and as time goes on, more and more segments of the chain are brought outside the original tube (in the directions both parallel and normal to its main axis). Eventually, the entire chain escapes. For the chain shown in Fig. 3, this happens after approximately 950 ns, which is comparable to the disentanglement time of the PE500 melt ($\approx$1040 ns), as estimated by the third break in the computed segmental msd curve [see, Fig. 1(a)].

In parts (a) and (b) of Fig. 4 we present values of the function $\psi(s,t)$ for $s=0$ or $s=1$ (corresponding to the two ends) and $s=0.5$ (corresponding to the middle segment) for a randomly selected PE500 chain, as a function of time. At very short times, we see that chain ends fluctuate rapidly in and out the original tube, since the value of the function $\psi(0,t)$ alternates rather quickly between 1 and 0. We also see that it takes approximately 6.7 ns for chain ends to completely escape the original tube. A similar picture characterizes the dynamics of the middle segment of the primitive chain, since this is also seen to fluctuate in and out the original tube. However, it takes this segment a significantly longer time, approximately equal to 615 ns (that is, almost two orders of magnitude longer), to completely escape!

The corresponding segment survival probability function $\psi(s,t)$ for the simulated melts accounting for all possible relaxation phenomena at length scales larger than the tube radius is shown in Fig. 5(a) for the PE systems and in Fig. 6(a) for the *cis*-PB systems. Its shape provides us with invaluable information for the time evolution of the primitive path conformation as chains diffuse due to thermal motion and under the application of intramolecular and intermolecular forces. For the very early times, most of the middle segments remain inside the initial tube, whereas many of the outer segments seem to have escaped (especially those closer to the two chain ends). Furthermore, the whole $\psi(s,t)$ curve is shown to decline to lower values with time, which corresponds to our expectation that more and more segments of the primitive chain tend to move out of the initial tube with time. On the average, the computed $\psi(s,t)$ curves are consistent with the conceptual reptation mechanism of the effec-

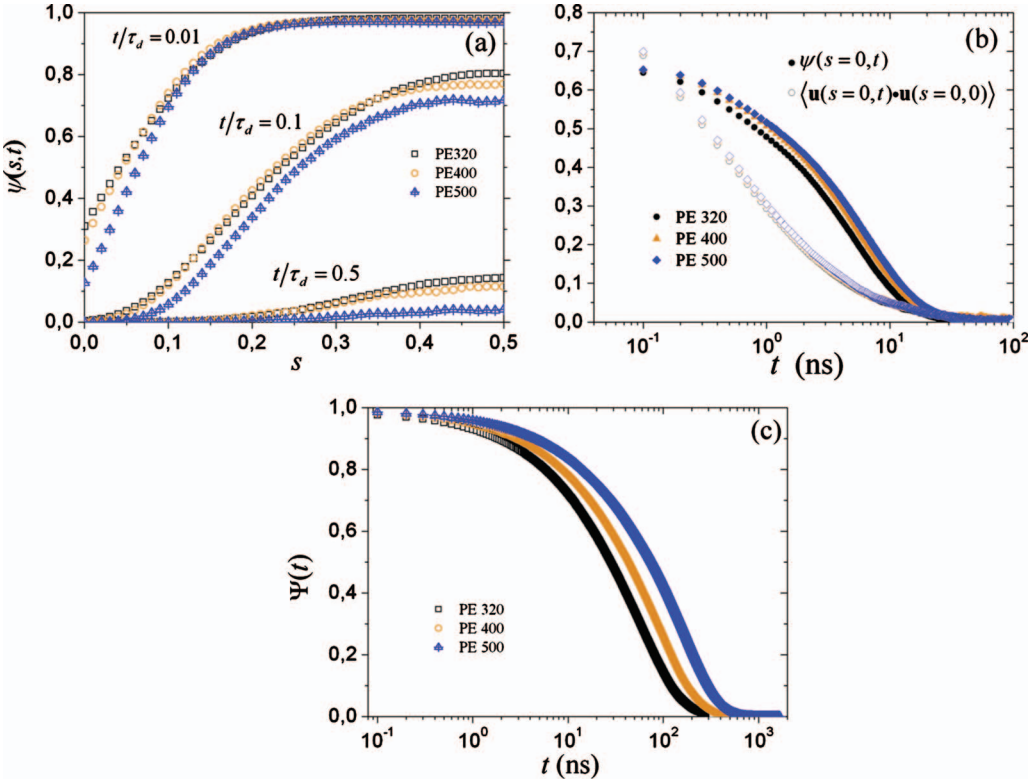

FIG. 5. Results from the present direct PP analysis for the simulated PE melts: (a) Typical plots of the function $\psi(s,t)$ describing the probability that a primitive segment s remains in the initial tube after time t. (b) Plots of computed $\psi(s=0,t)$ curves for chain ends (filled symbols) and comparison with the curves describing the time decay of the autocorrelation function $\langle \mathbf{u}(s=0,t)\cdot\mathbf{u}(s=0,0)\rangle$ of the unit tangent vector $\mathbf{u}$ for end segments (empty symbols). (c) Typical plots of the function $\Psi(t)\equiv\int_0^1\psi(s,t)ds$ representing the fraction of primitive chain that has remained in the initial tube after time t.

tive tube model: they describe a chain which diffuses along the tube, simultaneously entering new tube segments at the one end (the "head") and vacating segments at the other end (the "tail"). In addition to reptation, CLFs and CR mechanisms are also evident in the figure. We also note that, in contrast to the simple boundary condition of $\psi(s=0,t)=\psi(s=1,t)=0$ assumed in classical tube theories, the present results are in favor of a very small but definitely nonzero value for $\psi(s,t)$ at chain ends for a certain time, reflecting the fact that, on statistical average, chain ends do remain inside the original tube for a finite time interval as they are fluctuating rapidly over a distance equal to approximately the tube radius, as clearly shown in Fig. 4(a). This happens because as chain ends fluctuate or dangle for some (short but) nonzero time interval in and out the original tube, $\psi(s=0,t=0^+)$ or $\psi(s=1,t=0^+)$ cannot come out to be identically zero. They will be zero only after the end points have totally escaped the tube; and clearly this takes some time to happen. This explains the small nonzero values of $\psi(s,t=0^+)$ at chain ends. It also suggests that chain ends can hold some elasticity for some time. In contrast, in all analytical theories, the end condition is treated as a first-passage problem; thus $\psi(s,t=0^+)$ is considered (i.e., *assumed*) to be identically zero at chain ends (end segments are assumed to have a zero lifetime or to be replaced instantaneously). Our simulation results show this *not* to be exactly so. But, of course, for very long polymers, the time scale on which such end effects will persist will be relatively unimportant: the time for which $\psi(s,t=0^+)$ for chain ends will remain nonzero in these systems will be too small compared to their reptation time. In the literature, nonzero life times for chain ends have also been reported by Kröger–Hess[30] and Aoyagi–Doi[31] based on computations with a coarse-grained model for the polymer.

Additional insight into the dynamics of chain ends can be gained by comparing the $\psi(s=0,t)$ curves computed from the present PP analysis with the time decay curves of the autocorrelation function $\langle \mathbf{u}(s=0,t)\cdot\mathbf{u}(s=0,0)\rangle$ of the unit tangent vector $\mathbf{u}$ for end segments. As can be seen from the graphs reported in Figs. 5(b) and 6(b), although $\langle \mathbf{u}(s=0,t)\cdot\mathbf{u}(s=0,0)\rangle$ decays slightly faster than $\psi(s=0,t)$ at early times, both of them approach zero after practically the same time (for a given system). Furthermore, it is reassuring that the rates with which the two quantities drop to zero are nearly independent of the chain length, which emphasizes the fact that chain end dynamics should not depend on chain length (unless the chains are too short). In fact, by fitting the computed $\psi(0,t)$ or $\langle \mathbf{u}(s=0,t)\cdot\mathbf{u}(s=0,0)\rangle$ relaxation curves with stretched exponential (i.e., KWW) functions of the form[27]

$$\psi(0,t)=\psi(1,t)=A\,\exp[-(t/\tau_{\mathrm{KWW}})^{\beta_{\mathrm{KWW}}}] \tag{6a}$$

and

$$\langle \boldsymbol{u}(s=0,t)\cdot\boldsymbol{u}(s=0,0)\rangle=\langle \boldsymbol{u}(s=1,t)\cdot\boldsymbol{u}(s=1,0)\rangle = A\,\exp[-(t/\tau_{KWW})^{\beta_{KWW}}], \tag{6b}$$

respectively, we can have a direct estimate of the corresponding relaxation times, $\tau_c=A\tau_{\mathrm{KWW}}[\Gamma(1/\beta_{\mathrm{KWW}})/\beta_{\mathrm{KWW}}]$, for the

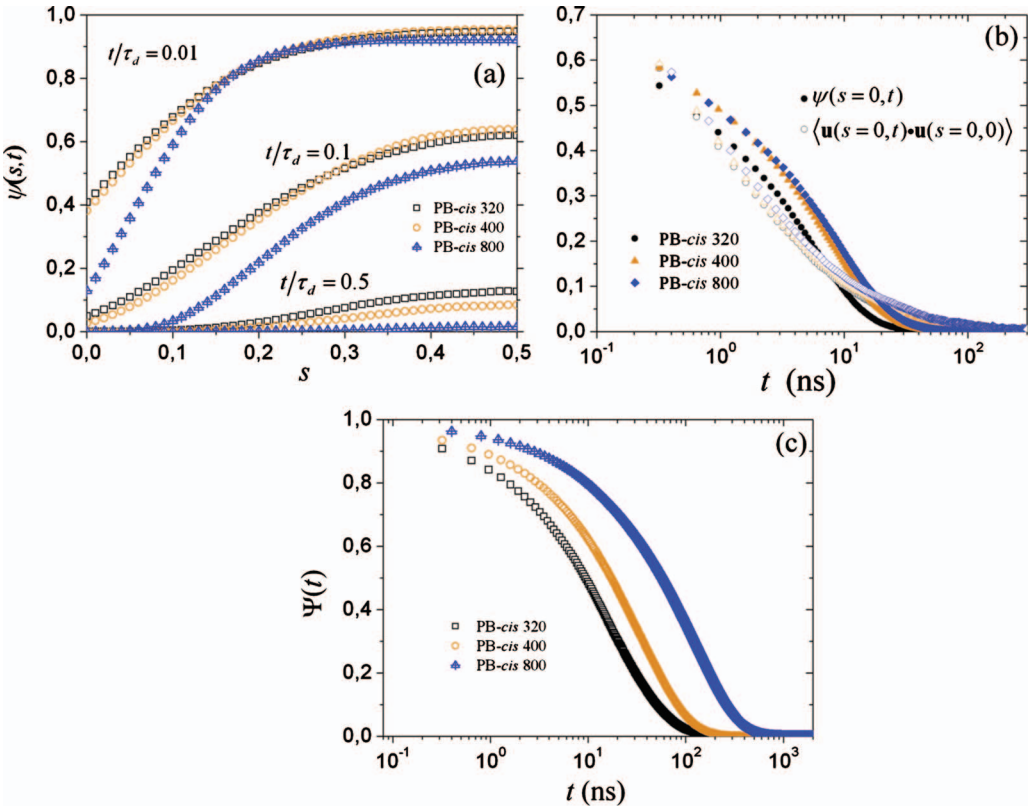

FIG. 6. Same as with Fig. 5 but for the PB-*cis* systems.

end segments; the results are shown in Table II. A careful investigation of the numerical results for τ_c reported in Table II from the two sets of curves, $\psi(0,t)$ versus t and $\langle \mathbf{u}(s=0,t)\cdot\mathbf{u}(s=0,0)\rangle$ versus t, for the three different simulated systems (PE, *cis*-1,4-PB and *trans*-1,4-PB) reveals that to a very good approximation these are for all practical purposes equal to the corresponding entanglements times τ_e reported in Table I. This is a significant result of the present work validating among others a recent proposition by van Rymbeke *et al.*[32] (that a time approximately equal to τ_e is needed before chain ends reach equilibrium) in an effort to resolve the so-called "time-stress discrepancy" of tube models when these are employed to describe the apparent plateau modulus of short, weakly entangled linear chains (despite the fact that they capture almost accurately their terminal relaxation behavior).

TABLE II. Values of the characteristic relaxation times τ_c describing the time decay of $\psi(0,t)$ and of $\langle \mathbf{u}(s=0,t)\cdot\mathbf{u}(s=0,0)\rangle$, Eqs. (6a) and (6b) in the main text.

System	τ_c (ns) from the decay of $\psi(0,t)$ or $\psi(1,t)$	τ_c (ns) from the decay of $\langle \mathbf{u}(s=0,t)\cdot\mathbf{u}(s=0,0)\rangle$ or $\langle \mathbf{u}(s=1,t)\cdot\mathbf{u}(s=1,0)\rangle$
PB-*cis*320	3.1	4.3
PB-*cis*400	4.4	5.4
PB-*cis*800	5.1	7.4
PB-*trans*320	5.2	6.8
PB-*trans*400	4.8	7.9
PE320	3.2	2.1
PE400	3.8	2.3
PE500	4.7	2.3

The segment survival probability function $\psi(s,t)$ is expected to be related to the life time of entanglements. Ideally, a single entanglement should be a binary contact involving only two chains, implying that in principle we should be able to compare the lifetimes of entanglements with the tube survival function. The Z1 code, however, does not provide a unique list of binary contacts. It allows one to define entanglements based solely on the shortest path information; as a result, "kinks" on one chain formed against a straight segment of another chain do not always result in topological constraints that are pairwise associated on the two chains. Binary entanglements are more conveniently identified in the contour reduction topological analysis (CRETA) algorithm proposed by Tzoumanekas and Theodorou.[17] We are currently extending the Z1 code so that it can also detect (geometrically) entanglement pairing. We hope to be able to report results on the relationship between the time decay of the $\psi(s,t)$ function and the entanglement lifetime along the chain contour from either of the two methods (Z1 and CRETA) in the near future.

Having computed $\psi(s,t)$ through the proposed PP analysis, various LVE properties can be extracted for the simulated systems. We consider first the function $\Psi(t)$ which represents the fraction of the primitive chain that has remained in the initial tube after time t. Since the computed $\psi(s,t)$ curves as obtained from the direct PP analysis already contain the CLF and CR effects, this defines also the (reduced) relaxation modulus $G(t)/G_N^0$ [see Eq. (1b) above]. The re-

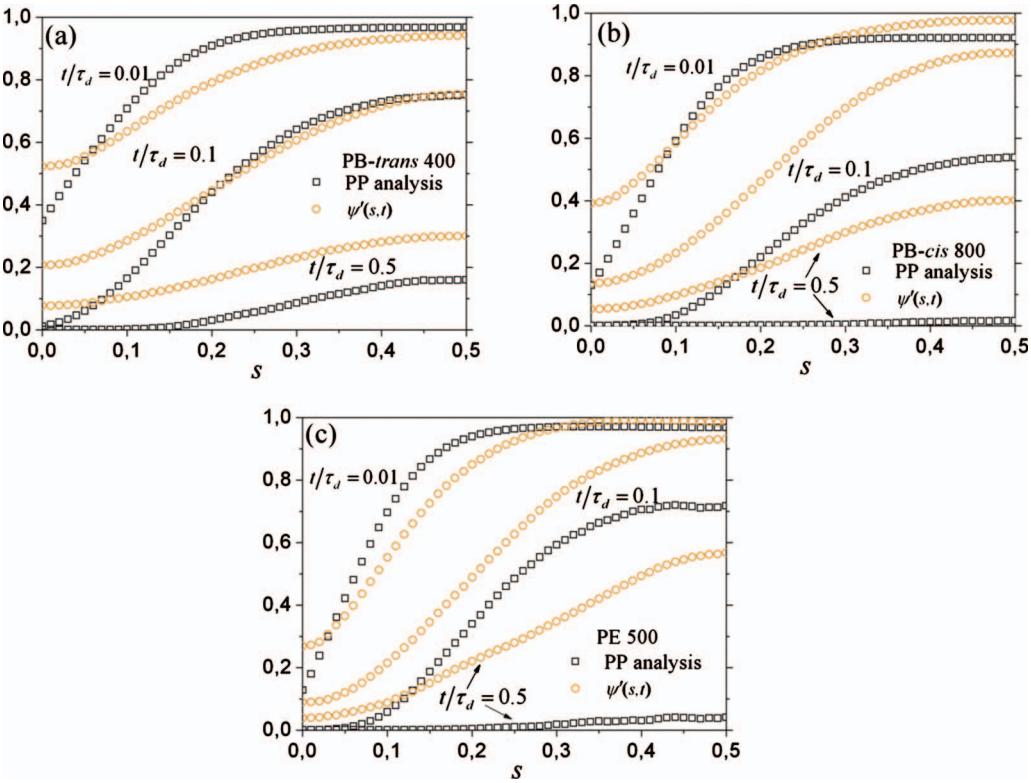

FIG. 7. Comparison of the function $\psi(s,t)$ giving the probability that the tube segment s is remaining in the tube after time t with the function $\psi'(s,t)$ describing the correlation of the tangent vectors **u** along the primitive chain, Eq. (5a) in the main text. The results have been obtained from the simulations with the PB-*trans*400 (a), PB-*cis*800 (b), and PE500 (c) melts.

sults obtained for the function $\Psi(t)$ are reported in Fig. 5(c) for the simulated PE melts and in Fig. 6(c) for the simulated *cis*-PB systems.

As discussed at the end of Sec. II, based on the original Doi–Edwards theory, the segment survival probability function $\psi(s,t)$ in the absence of CR comes out to be equal to the function $\psi'(s,t)$ describing the correlation of the tangent vectors along the PP. We have computed the function $\psi'(s,t)$ for all systems simulated here and the curves obtained, together with the $\psi(s,t)$ curves that we computed from the direct PP analysis, are plotted in Fig. 7. The plots indicate a faster relaxation of the $\psi(s,t)$ curves which is a direct consequence of CR effects: By releasing topological constraints along the chain, CR accelerates chain relaxation especially at the middle points, without significantly affecting the degree of the time decay of the chain end-to-end vector autocorrelation function. As a result, the $\psi(s,t)$ curves fall always faster than the corresponding $\psi'(s,t)$ curves.

In Fig. 8 we show a comparison of the $\Psi(t)$ plots (corresponding to the PB-*trans*400, PE320, and PB-*cis*800 systems) obtained from the three different methods discussed above: (i) the average fraction of the primitive chain that has remained in the initial tube after time t [Eq. (1a)]; i.e., directly from our topological analysis by integrating the computed $\psi(s,t)$ function, (ii) the simplified Green–Kubo relationship based on Eqs. (2) and (4), and (iii) the time autocorrelation function $\Psi'(t)$ of the chain end-to-end vector [Eq. (5)] which describes reptation in the absence of CR. Good agreement between methods (i) and (iii) is observed for all three systems only at the very early times. At later times, $\Psi(t)$ as computed by the direct PP analysis relaxes faster than the autocorrelation function $\Psi'(t)$ of the chain end-to-end vector, indicating once again that CR effects make a significant contribution to the (stress) relaxation, especially for middle segments. On the other hand, the Green–Kubo method, method (ii), results in $G(t)/G_N^0$ values that suggest a faster melt relaxation at early and intermediate time scales than the other two methods; considering, however, the assumptions behind Eq. (4) for the form of the employed Green–Kubo relationship, the overall prediction is not bad at all. In fact, it is very interesting that the predictions of the Green–Kubo relationship at longer times are quantitatively more consistent with the direct PP analysis of method (i) than those based on the time autocorrelation function of the chain end-to-end vector, $\Psi'(t)$, which neglects CR.

As noted above, using $G(t)=G_N^0\Psi(t)$ (keeping in mind that it is only valid for times t longer than the characteristic time τ_e that chain segments "hit" the tube), we can calculate other important LVE properties such as the zero-shear viscosity η_0, the steady-state compliance J_e^0, and the storage and loss moduli, $G'(\omega)$ and $G''(\omega)$, respectively. Figure 9 compares the zero shear rate viscosities obtained from our PP analysis with reported experimental data[33–37] for a number of model PE [Fig. 9(a)] and PB [Fig. 9(b)] melts. For both polymers and for all chain length systems studied, the agreement is considered to be quite satisfactory. For the PB systems, in particular, we should take into account that the experimental samples are not entirely 100% *cis*-1,4 or 100% *trans*-1,4 but they contain a significant percentage of *vinyl*

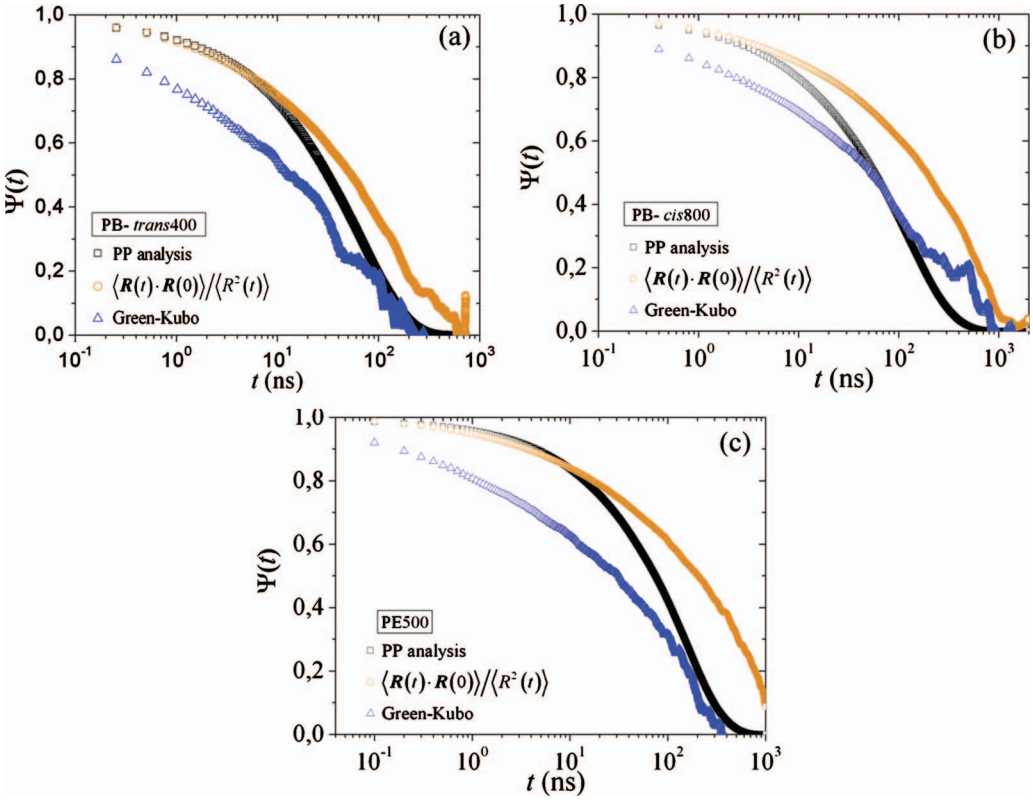

FIG. 8. Computed relaxation curves for the PB-*trans*400 (a), PB-*cis*800 (b), and PE500 (c) melts, from the three different methods discussed in the main text: (i) the proposed topological analysis that leads self-consistently to the computation of the $\psi(s,t)$ function, (ii) the coarse-grained version of the Green–Kubo expression [Eqs. (2) and (4)], and (iii) the time autocorrelation function of the chain end-to-end vector [Eq. (5b)]; the latter describes stress relaxation in the absence of CR.

and 1,2-*trans* or 1,2-*cis* comonomer. Despite this, the computed values seem to fall not too far away from the measured ones. These first encouraging results justify the relevance of the proposed methodology for mapping simulation trajectories onto the tube model and are in support of the basic tube model picture for the dynamics of chains in entangled polymers.

IV. CONCLUDING REMARKS

In summary, we have presented a systematic methodology that enables one to extract the primary ingredient of all tube theories for entangled polymer melts, the segment-survival probability function $\psi(s,t)$, through a direct topological analysis of atomistic simulation data and dynamical mapping of the resulting chain trajectories onto the tube model. This complements recent contributions in the field[14–17] where only the static (statistical) properties of the PP network were addressed. Predicted LVE properties for various PE and PB melts with the new methodology have been observed to be consistent with rheological data from independent experimental measurements. PP reptation longitudinally inside the tube as well as local transverse fluctuations of the chain driven mainly from constraint release and regeneration mechanisms have been recorded in the simulation results. Additional results from the new approach for longer-chain systems and a detailed comparison with the functions $\psi(s,t)$ proposed by state-of-the-art models in the literature are currently in progress. We mention, for example,

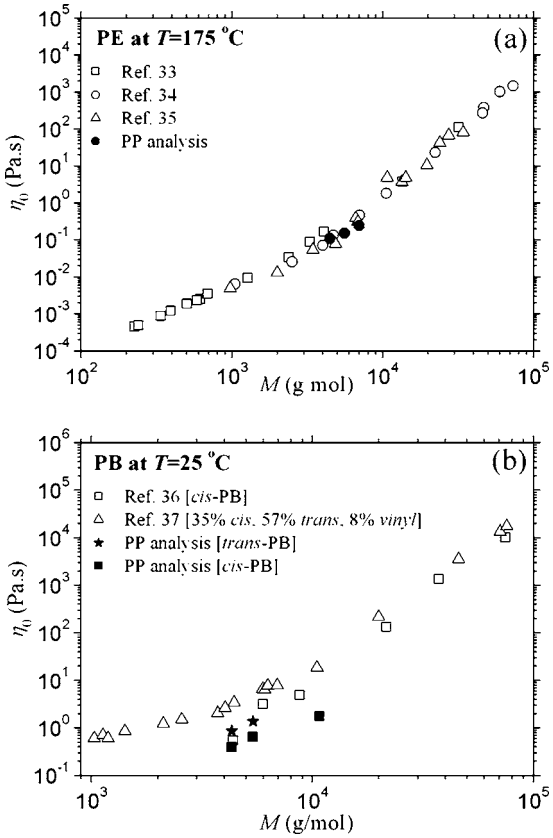

FIG. 9. The zero-shear viscosity as obtained from the present PP analysis for: (a) linear PE melts and (b) linear *cis*- and *trans*-PB melts, and comparison with reported experimental data.

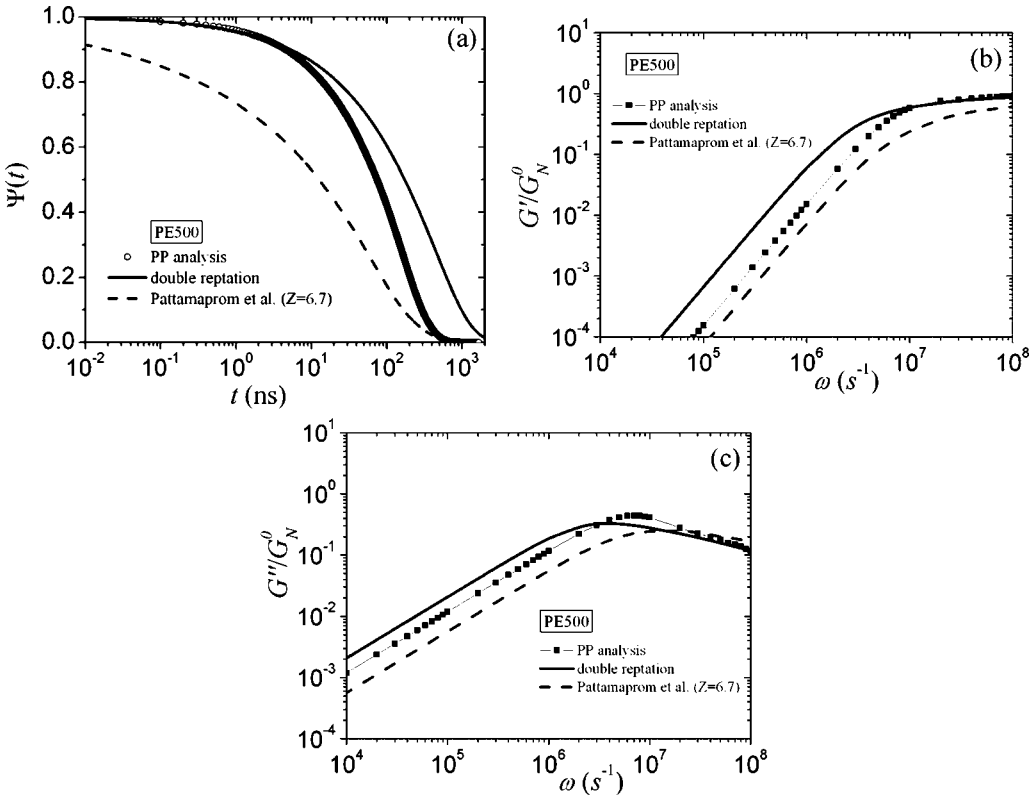

FIG. 10. Comparison of the results obtained from the direct PP analysis with the computed $\psi(s,t)$ curves for the overall probability $\Psi(t)=G(t)/G_N^0$ (a), the spectra of storage $G'(\omega)$ (b), and loss $G''(\omega)$, (c) moduli of the PE500 melt with the double constraint (Ref. 38) and dual constraint (Refs. 42 and 43) models.

the dynamic dilution models according to which $\Psi(t)=\mu(t)^{\alpha+1}$ ($\alpha=1$ for double reptation[38] whereas Colby and Rubinstein[39] propose $\alpha=4/3$), the Rubinstein–Colby model[40] built on the postulate of Graessley[41] that $\Psi(t)$ should be factorized as $\Psi(t)=\mu(t)R(t)$ where $\mu(t)$ accounts for reptation and CLF while $R(t)$ which accounts for CR should be calculated in a self-consistent way from $\mu(t)$, the Pattamaprom *et al.*[42,43] model where an additional reaction-type term is added to the Doi–Edwards evolution equation for $\psi(s,t)$, and the Leygue *et al.*[44] model where the diffusion coefficient is position-dependent. These comparisons will be very useful in: (a) evaluating existing tube-based theories accounting for CLF and CR effects, branching and polydispersity in chain length, and (b) proposing suitable modifications and refinements based on atomistic-level information; they will be reported in a future publication. For example, in Fig. 10, we report results from our PP analysis for the function $\Psi(t)(=G(t)/G_N^0)$ and the spectra of storage and loss moduli, $G'(\omega)$ and $G''(\omega)$, of the PE500 system (the longest polymer simulated here) and compare them with the predictions of the double reptation[38] and dual constraint[42,43] models. The dual constraint model has been proposed by Pattamaprom *et al.*[42,43] by considering both shallow (τ_{early}) and deep (τ_{late}) fluctuations[45] (see Pattamaprom *et al.*[43] for corrections in some of the numerical prefactors following Larson *et al.*[46]) and by adding a "reaction" term to the partial differential equation (PDE) of the Doi–Edwards model (the simple diffusion equation) in order to account for CLF effects. The mathematical equations describing the dual constraint model are given in the Appendix. In the Appendix, we also report the expression for the relaxation modulus describing the double reptation model. For the comparison with the double constraint model in Fig. 10 we used $\tau_d=1042$ ns while for the comparison with the dual reptation model we used $\tau_R=125\pm20$ ns, $\tau_d=1042\pm46$ ns, and $Z=6.7$ (corresponding to a value of $N_e=74$ for the entanglement length); all these parameter values have been extracted directly from the atomistic MD simulations and the subsequent PP analysis carried out in the present work. Part (a) of the figure compares the three sets of data at the level of the overall probability $\Psi(t)=G(t)/G_N^0$ while parts (b) and (c) extend the analysis to the level of the storage $G''(\omega)$ and loss $G''(\omega)$ moduli, respectively. The comparison has been restricted to low frequencies (corresponding to times longer than the entanglement time τ_e) and is very favorable since all three sets of data (direct simulation, double reptation model, and dual constraint model) are seen to be qualitatively very similar, with the curves obtained from the direct PP analysis falling in all cases in between the curves corresponding to the two theoretical models. The comparison verifies that the double reptation model overestimates somewhat the data obtained from the direct PP analysis, something that should have been expected given that no CLF corrections are included in this model. On the other hand, that the predictions of the dual constraint model are below those of the direct PP analysis seems to suggest that, for the simulated system (PE500 melt), CLF effects as computed with the help of Eq. (A1b) in the Appendix are probably overestimated. As we mentioned above, in a future effort we will extend the comparison to include other models as well; we will also try to simulate and

analyze longer polymer melts (e.g., a C_{1000} PE melt) which will allow for a more direct comparison with the theoretical models which by default are designed to describe the viscoelasticity of truly long polymer melts.

By providing the link between microscopic level simulations and macroscopic phenomenological models, the new approach (in conjunction with state-of-the-art nonequilibrium MD simulations of polymers in shear[47] and planar elongation[48]) can also address systems subjected to flow. Establishing our concept under nonequilibrium conditions would mark a tremendous achievement, since it could help quantify the effect and role of other mechanisms (such as CCR[49,50]) on the linear and nonlinear viscoelastic properties of polymers. In conjunction with the design of thermodynamically consistent coarse-graining methodologies for systems beyond equilibrium,[51–55] this could enable the prediction of the rheological properties of truly long polymers and the development of more accurate constitutive equations based on multiscale constructions (involving, e.g., projection operators) in the framework of nonequilibrium statistical mechanics and thermodynamics.

ACKNOWLEDGMENTS

We would like to express our gratitude to the anonymous referee who found fundamental errors in the originally submitted version of this work, without the correction of which the conclusions drawn from our PP computations would have been grossly misleading. We are grateful to the authors of Ref. 36 for making available to us their viscosity data for the PB melt shown in Fig. 9 prior to publication, to Dr. E. van Ruymbeke for many helpful discussions, and to Dow Benelux B.V. (especially to Dr. J. Storer, Dr. J. den Doelder, and Dr. R. Koopmans) for financial support and the allocation of central processing unit time on their supercomputing center in the course of this work. M.K. has been supported by the Swiss National Science Foundation through grant IZ73Z0-128169.

APPENDIX: DUAL CONSTRAINT MODEL

The dual constraint model is constructed in two stages. In stage 1, the PDE considered is

$$\frac{\partial}{\partial t}\psi^*(s,t) = \frac{D_c}{\langle L\rangle^2}\frac{\partial^2}{\partial s^2}\psi^*(s,t) - \frac{1}{\tau^*(s)}\psi^*(s,t), \tag{A1a}$$

where

$$\tau_{\text{early}}(s) = \frac{9}{16}\pi^3\frac{\tau_R}{c^4}Z^2(1-cs)^4,$$

$$\tau^*_{\text{late}}(s) = \frac{\tau_R}{c^2}\exp[U^*(s)], \tag{A1b}$$

$$U^*(s) = \frac{3}{2}Z(1-cs)^2,$$

with $c=2$ for a linear chain. We may also use the reptation time $\pi^2\tau_d = D_c/\langle L\rangle^2$. Then $\tau^*(s)$, which is needed in Eq. (A1a), is obtained simply as[42,43]

$$\tau_{\text{early}}(s) = \begin{cases} \tau_{\text{early}}(s) & (1-cs) < C_1 \\ \sqrt{\tau_{\text{early}}(s)\tau^*_{\text{late}}(s)} & C_1 < (1-cs) < C_2 \\ \tau^*_{\text{late}}(s) & (1-cs) < C_2 \end{cases}, \tag{A1c}$$

where C_1 denotes the first crossover position of τ_{early} to τ_{late} close to chain ends $(1-cs=0)$ and C_2 the second crossover position of τ_{late} to τ_{early} deeper inside the tube. Solving PDE [Eq. (A1a)] gives also the overall probability $\phi^*(t) = \int_0^1 ds\psi^*(s,t)$. Finally, an expression for the approximate Rouse process is used; this Rouse process is activated whenever $\phi^*(t)$ decreases faster than the Rouse process. Pattamaprom *et al.*[42,43] used the expression proposed by Milner and McLeish,[45] namely

$$\phi^*_R(t) = \phi^*(t=t_0)\left(\frac{t}{t_0}\right)^{-1/2}, \tag{A1d}$$

where t_0 denotes the time beyond which $\phi^*(t)$ starts to decrease faster than $t^{-1/2}$. The expression for the average probability $\Phi^*(t)$ is taken then as

$$\Phi^*(t) = \begin{cases} \phi^*(t) & \text{if } \phi^*(t) > \phi^*_R(t) \\ \phi_R(t) & \text{if } \phi^*(t) < \phi^*_R(t) \end{cases}. \tag{A1e}$$

In stage 2, CR is also taken into account by including $\Phi^*(t)$ into the deep fluctuations by considering the following PDE:

$$\frac{\partial}{\partial t}\psi(s,t) = \pi^2\tau_d\frac{\partial^2}{\partial s^2}\psi(s,t) - \frac{1}{\tau(s)}\psi(s,t), \tag{A2a}$$

where τ_{early} is the same as in Eq. (A1b) but now

$$\tau_{\text{late}}(s) = \frac{\tau_R}{c^2}\exp[U(s)],$$

$$U(s) = \frac{3}{2}Z\Phi^*(t)(1-cs)^2. \tag{A2b}$$

On the other hand, $\tau(s)$ is obtained in a way which is completely analogous to that in stage 1 as[42,43]

$$\tau_{\text{early}}(s) = \begin{cases} \tau_{\text{early}}(s) & (1-cs) < C_1(t) \\ \sqrt{\tau_{\text{early}}(s)\tau_{\text{late}}(t,s)} & C_1(t) < (1-cs) < C_2(t) \\ \tau_{\text{late}}(t,s) & (1-cs) < C_2(t) \end{cases}, \tag{A2c}$$

with the crossover positions now depending on time through the inclusion of $\Phi^*(t)$ into the activation energy. Solving the PDE gives also the overall probability $\phi(t) = \int_0^1 ds\psi(s,t)$. Using the Rouse process[45]

$$\phi_R(t) = \phi(t=t_0)\left(\frac{t}{t_0}\right)^{-1/2}, \tag{A2d}$$

where t_0 is the time when $\phi(t)$ starts to decreases faster than $t^{-1/2}$, the expression for the average probability $\Phi(t)$ is given, in a similar manner, as

$$\Phi(t) = \begin{cases} \phi(t) & \text{if } \phi(t) > \phi_R(t) \\ \phi_R(t) & \text{if } \phi(t) < \phi_R(t) \end{cases}. \tag{A2e}$$

The overall survival probability $\Psi(t)$, which enters the calculation of the relaxation modulus through $G(t)=G_N^0\Psi(t)$, is finally obtained by multiplying $\Phi(t)$ with $\Phi^*(t)$ (Refs. 42 and 43)

$$\Psi(t) = \Phi^*(t)\Phi(t). \tag{A2f}$$

For completeness, we also note that the double reptation model is obtained by choosing in Eq. (A2f)

$$\Phi^*(t) = \Phi(t) = \sum_{p:\text{odd}}^{\infty} \frac{8}{p^2\pi^2} \exp\left[-p^2\frac{t}{\tau_d}\right]. \tag{A3}$$

[1] M. Doi and S. F. Edwards, *The Theory of Polymer Dynamics* (Clarendon, Oxford, 1986).
[2] P. G. de Gennes, J. Chem. Phys. **55**, 572 (1971).
[3] M. Doi and S. F. Edwards, J. Chem. Soc., Faraday Trans. 2 **74**, 1789 (1978); **74**, 1802 (1978); **74**, 1818 (1978).
[4] D. Richter, B. Farago, L. J. Fetters, J. S. Huang, B. Ewen, and C. Lartigue, Phys. Rev. Lett. **64**, 1389 (1990).
[5] J. Noolandi, G. W. Slater, H. A. Lim, and J. L. Viovy, Science **243**, 1456 (1989).
[6] S. D. Levene and B. H. Zimm, Science **245**, 396 (1989).
[7] T. C. B. McLeish, Adv. Phys. **51**, 1379 (2002).
[8] T. P. Lodge, Phys. Rev. Lett. **83**, 3218 (1999).
[9] M. Doi, J. Polym. Sci., Polym. Phys. Ed. **21**, 667 (1983).
[10] J. des Cloizeaux, J. Phys. (France) Lett. **45**, 17 (1984).
[11] R. J. Needs, Macromolecules **17**, 437 (1984).
[12] H. Watanabe, Prog. Polym. Sci. **24**, 1253 (1999).
[13] H. Watanabe, S. Ishida, Y. Matsumiya, and T. Inoue, Macromolecules **37**, 6619 (2004).
[14] R. Everaers, S. K. Sukumaran, G. S. Grest, C. Svaneborg, A. Sivasubramanian, and K. Kremer, Science **303**, 823 (2004).
[15] M. Kröger, Comput. Phys. Commun. **168**, 209 (2005).
[16] K. Foteinopoulou, N. C. Karayiannis, V. G. Mavrantzas, and M. Kröger, Macromolecules **39**, 4207 (2006).
[17] C. Tzoumanekas and D. N. Theodorou, Macromolecules **39**, 4592 (2006).
[18] R. N. Khaliullin and J. D. Schieber, Phys. Rev. Lett. **100**, 188302 (2008).
[19] S. Shanbhag and M. Kröger, Macromolecules **40**, 2897 (2007).
[20] M. Doi, J. Phys. A **8**, 959 (1975).
[21] M. Rubinstein and E. Helfand, J. Chem. Phys. **82**, 2477 (1985).
[22] M. Mondello and G. S. Grest, J. Chem. Phys. **106**, 9327 (1997).
[23] V. A. Harmandaris, V. G. Mavrantzas, and D. N. Theodorou, Macromolecules **33**, 8062 (2000).
[24] N. C. Karayiannis and V. G. Mavrantzas, Macromolecules **38**, 8583 (2005).
[25] G. Tsolou, V. G. Mavrantzas, and D. N. Theodorou, Macromolecules **38**, 1478 (2005).
[26] H. C. Öttinger, J. Non-Newtonian Fluid Mech. **120**, 207 (2004).
[27] J. D. Ferry, *Viscoelastic Properties of Polymers* (Wiley, New York, 1980).
[28] L. J. Fetters, D. J. Lohse, D. Richter, T. A. Witten, and A. Zirkel, Macromolecules **27**, 4639 (1994).
[29] L. J. Fetters, D. J. Lohse, S. Milner, and W. W. Graessley, Macromolecules **32**, 6847 (1999).
[30] M. Kröger and S. Hess, Physica A **195**, 336 (1993).
[31] T. Aoyagi and M. Doi, Comput. Theor. Polym. Sci. **10**, 317 (2000).
[32] E. van Ruymbeke, D. Vlassopoulos, M. Kapnistos, C. Y. Liu, and C. Bailly, Macromolecules **43**, 525 (2010).
[33] D. S. Pearson, G. V. Strate, E. von Meerwall, and F. C. Schilling, Macromolecules **20**, 1133 (1987).
[34] D. S. Pearson, L. J. Fetters, W. W. Graessley, G. Strate, and V. E. von Meerwall, Macromolecules **27**, 711 (1994).
[35] V. A. Harmandaris, V. G. Mavrantzas, D. N. Theodorou, M. Kröger, J. Ramírez, H. C. Öttinger, and D. Vlassopoulos, Macromolecules **36**, 1376 (2003).
[36] M. Kapnistos, E. van Ruymbeke, and D. Vlassopoulos (private communication).
[37] R. H. Colby, L. J. Fetters, and W. W. Graessley, Macromolecules **20**, 2226 (1987).
[38] J. L. Viovy, J. Phys. (France) **46**, 847 (1985); G. Marrucci, J. Polym. Sci., Polym. Phys. Ed. **23**, 159 (1985); C. Tsenoglou, Polym. Prepr. (Am. Chem. Soc. Div. Polym. Chem.) **28**, 185 (1987); J. des Cloizeaux, Europhys. Lett. **5**, 437 (1988).
[39] R. H. Colby and M. Rubinstein, Macromolecules **23**, 2753 (1990).
[40] M. Rubinstein and R. H. Colby, J. Chem. Phys. **89**, 5291 (1988).
[41] W. W. Graessley, Adv. Polym. Sci. **47**, 67 (1982).
[42] C. Pattamaprom, R. G. Larson, and T. J. Van Dyke, Rheol. Acta **39**, 517 (2000); C. Pattamaprom and R. G. Larson, *ibid.* **40**, 516 (2001).
[43] C. Pattamaprom, R. G. Larson, and A. Sirivat, Rheol. Acta **47**, 689 (2008).
[44] A. Leygue, C. Bailly, and R. Keunings, J. Non-Newtonian Fluid Mech. **133**, 28 (2006).
[45] S. T. Milner and T. C. B. McLeish, Macromolecules **30**, 2159 (1997); Phys. Rev. Lett. **81**, 725 (1998).
[46] R. G. Larson, T. Sridhar, L. G. Leal, G. H. McKinley, A. E. Likhtman, and T. C. B. McLeish, J. Rheol. **47**, 809 (2003).
[47] D. J. Evans and G. P. Morriss, *Statistical Mechanics of Nonequilibrium Liquids* (Academic, London, 1990).
[48] C. Baig, B. J. Edwards, D. J. Keffer, H. D. Cochran, and V. A. Harmandaris, J. Chem. Phys. **124**, 084902 (2006).
[49] G. Marrucci, J. Non-Newtonian Fluid Mech. **62**, 279 (1996).
[50] G. Ianniruberto and G. Marrucci, J. Non-Newtonian Fluid Mech. **65**, 241 (1996).
[51] C. Pierleoni, C. Addison, J.-P. Hansen, and V. Krakoviack, Phys. Rev. Lett. **96**, 128302 (2006).
[52] M. Gell-Mann and J. B. Hartle, Phys. Rev. A **76**, 022104 (2007).
[53] P. Ilg, H. C. Öttinger, and M. Kröger, Phys. Rev. E **79**, 011802 (2009).
[54] C. Baig and V. G. Mavrantzas, Phys. Rev. Lett. **99**, 257801 (2007).
[55] C. Baig and V. G. Mavrantzas, Phys. Rev. B **79**, 144302 (2009).